Proceedings of the 8th U.S. National Conference on Earthquake Engineering
April 18-22, 2006, San Francisco, California, USA
Paper No. 1452

NONLINEAR FINITE ELEMENT ANALYSIS OF DRILLED PIERS UNDER DYNAMIC AND STATIC AXIAL LOADING

Gang Wang [1] and Nicholas Sitar [2]

ABSTRACT

Realistic time history simulation of drilled pier/pile-soil system under dynamic and static loading is essential for development of effective performance based earthquake design of deep foundations. In this paper, we present the results of numerical simulation of a series of static and dynamic tests on drilled piers that were performed at UC Berkeley. We implemented a nonlinear soil model based on multi-axial cyclic bounding surface plasticity within a general finite element framework OpenSees ©. The model requires a minimal number of parameters that can be easily obtained through conventional site investigations. The results of the simulations show that the model can reasonably capture modulus reduction and hysteretic damping, the nonlinear response of the soil, and the model is suitable for fully nonlinear analysis of soil-pile system under multi-directional shaking. Most importantly, the model does a good job of capturing the actual load deformation curves obtained from the in-situ dynamic and static pier load tests.

Introduction

In the past, much effort has been devoted to the study of lateral response of the pile-soil systems, but very few studies have addressed their axial response. Yet, as schematically illustrated in Fig. 1, vertically propagated shear wave during an earthquake causes rocking of the structure, which subsequently induces vertical up-and-down axial movement of piles. Similar phenomenon is also commonly experienced by oil platforms subjected to wave/storm loads. In particular, earthquake loading rate is about three orders of magnitude greater than the rate for which the static pile capacity is based. As observed from a series of prototype pier load tests recently performed on UC Berkeley campus, stiffness and capacity of pile-soil

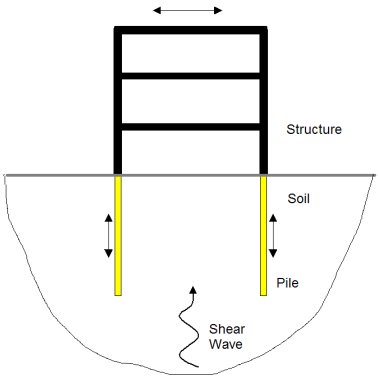

Figure 1. Foundation-soil-structure system.

[1] Graduate Research Assistant, Dept. of Civil and Environ. Eng., University of California, Berkeley, CA 94720
[2] Professor, Dept. of Civil and Environ. Eng., University of California, Berkeley, CA 94720

system shows great dependence on rate of loading and soil properties (Wang, 2005). Thus, for earthquake design of pile foundations, proper consideration of loading rate for piles may have important economic and safety implications (Kraft *et. al*, 1981).

Due to the nonlinear transient nature of the system and high computational requirements, to-date the application of nonlinear finite element analysis to this problem has been limited. Thus, an important aspect of numerical modeling is a soil model that is simple enough to be computationally efficient, yet able to capture the cyclic stress strain behavior. In particular, it is essential to account for the modulus degradation and energy dissipation characteristics during cyclic loadings, which depend on rate of loading and soil properties; Moreover, the model should have the potential to be used in three dimensional wave propagation and soil-foundation-structure interaction analysis. In this paper, we present a nonlinear soil model implementation based on multi-axial cyclic bounding surface plasticity and its validation through simulation of field tests on prototype drilled piers subjected to static and dynamic axial loading.

Constitutive Model for Cyclic Soil Response

Since early 1970's, many different nonlinear constitutive models of soil behavior were developed for various applications (see Zienkiewicz *et. al* 1999, Potts and Zdravkovic 1999, 2001). Motivated by the need for a smooth evolution of nonlinearity, Borja and Amies (1994) proposed a bounding surface plasticity model, called multi-axial cyclic plasticity model for cyclic clay behavior, which has been effectively utilized in *total stress* analyses of seismic site responses (e.g. Borja 1999a, 1999b, 2000; Rodriguez-Marek 2000). However, all these pervious studies considered only small strain soil behavior. For example, the mobilized maximum shear strain of soils in Borja (1999a) was only in an order of 0.2 %. To the authors' knowledge, this type of model has not been used in the analysis of strongly kinematically coupled problems, such as the pile-soil-structure system.

The basic concept of bounding surface plasticity is that there is no purely elastic region in the stress-strain relationship, instead, the nonlinearity of the soil is modelled by smoothly transforming the tangential shear modulus from small strain modulus to full plastic state through a state dependent hardening modulus. A stress function, called **bounding surface** $\mathcal{B}$, is used to specify the full plastic state. For clays under undrained condition, the bounding surface is assumed pressure independent, which is circular if viewed in the deviatoric stress plane (π plane). The radius of the circle can be determined from the ultimate strength parameter, such as undrained shear strength S_u. The rate form of constitutive relationship can be written as

$$\dot{\boldsymbol{\sigma}}' = 2G\,\dot{\boldsymbol{\varepsilon}}' = 2G_{\max}\left(1+\frac{3G_{\max}}{H'}\right)^{-1}\dot{\boldsymbol{\varepsilon}}' \tag{1}$$

where $\boldsymbol{\sigma}'$ is the deviatoric stress and $\boldsymbol{\varepsilon}'$ is the deviatoric strain, with prime used here to denote they are *deviatoric* tensors. G is tangential shear modulus, $G_{\max}$ is the maximum shear modulus at small strain and H' is a hardening modulus depending on the position of current stress point.

Given a most recent stress reversal point $\boldsymbol{\sigma}'_0$, the current deviatoric stress $\boldsymbol{\sigma}'$ and its image

point $\hat{\boldsymbol{\sigma}}'$ on the bounding surface $\mathcal{B}$, see Fig. 2(a), a dimensionless scalar κ can be defined to measure the relative distance of these stress points

$$\kappa = \frac{\hat{\boldsymbol{\sigma}}' - \boldsymbol{\sigma}'}{\boldsymbol{\sigma}' - \boldsymbol{\sigma}'_0} \tag{2}$$

Accordingly, the hardening modulus H' is determined via a smooth function of κ. One example of such a function can be chosen as the exponential form as the following

$$H' = h\kappa^m + H_0 \tag{3}$$

in which h is a modulus parameter and m is a dimensionless scalar. H_0 is the kinematic hardening modulus for translation of the bounding surface in the stress space. It is worth pointing out that contours of constant H', termed as *contour surface* $\mathcal{F}$ in short, are also circular in π plane, as shown in Fig. 2(a). Using Eq. (3), the soil behaves instantaneously elastic around stress reversal point (i.e. $H' \to \infty$ and $G \to G_{\max}$ as $\boldsymbol{\sigma}' \to \boldsymbol{\sigma}'_0$), and transits asymptotically towards fully plastic stage on the bounding surface (where $H' = H_0$). The exponential parameters h and m control the rate of shear modulus degradation, and they can be determined by curve fitting the measured modulus degradation curve.

Identification of loading/unloading is critical for the cyclic material model. As interpreted geometrically in Fig. 2(b), the soil is undergoing *loading* if the deviatoric strain increment $\dot{\boldsymbol{\varepsilon}}'$ points outward from the contour surface $\mathcal{F}$; *unloading* if $\dot{\boldsymbol{\varepsilon}}'$ points inward; and *neutral loading* if $\dot{\boldsymbol{\varepsilon}}'$ is tangential to $\mathcal{F}$. The criterion can be expressed by inner product (double contraction) of $\dot{\boldsymbol{\varepsilon}}'$ and the out normal tensor $\mathbf{n}$ of $\mathcal{F}$ as the following

$$\chi = \mathbf{n} : \dot{\boldsymbol{\varepsilon}}' \begin{cases} > 0, & \text{loading} \\ = 0, & \text{neutral loading} \\ < 0, & \text{unloading} \end{cases} \tag{4}$$

Once the unloading is identified, all previous $\mathcal{F}$ surfaces dissolve. Stress reversal point $\boldsymbol{\sigma}'_0$ is updated to the new stress unloading point (which coincides with $\boldsymbol{\sigma}'$ upon just unloading), and new $\mathcal{F}$ surfaces for constant hardening modulus H' are re-centered about the new position to interpolate the subsequent *loading* process. Fig. 2(c) illustrates a complete loading-unloading-reloading response.

In summary, the model requires minimal parameters that can be easily calibrated through a conventional field investigation, and the model can capture most important aspect of dynamic simulation, namely, the modulus reduction and energy dissipation. The recommended methods to calibrate model parameters are listed in Table 1.

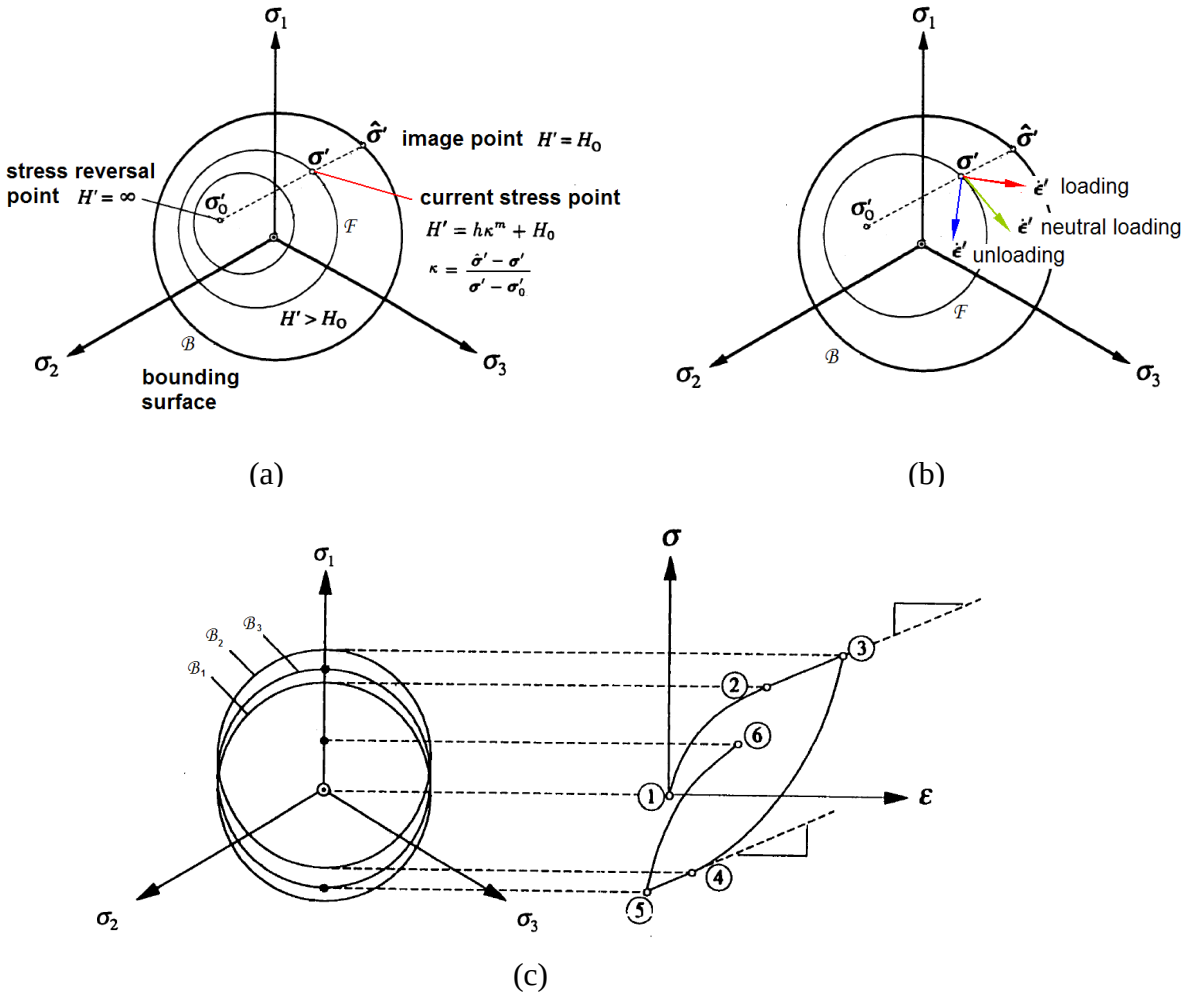

Figure 2. Cyclic soil model (a) bounding surface mapping rule (b) loading/unloading criterion (c) loading-unloading and reloading response.

Table 1. Determination of Model Parameters.

Model Parameters		**Calibration Methods**
Elastic Parameters	$G_{\max}$	Compute from shear wave velocity profile, $G_{\max} = \rho V_s^2$
	ν	Poisson's ratio
Strength Parameter	S_u	From unconfined compression test or SPT correlation
Hardening Parameters	h, m	Fit modulus reduction curves
	H_0	Fit tangential shear modulus at large strain

Simulation of Axial Pier Response

The above constitutive relationship was implemented in OpenSees© finite element framework in order to simulate a series of full-scale load tests on drilled piers. The test site is located at south of University of California Berkeley campus, and is mainly underlain by hard to very stiff sandy clay, medium dense sandy silt and dense clayey sand. All test piers were cast-in-place concrete piers, with dimension of 20 ~ 30 ft (6.1 ~ 9.1 m) long and 24 ~ 30 inches (0.61~ 0.76 m) in diameter. A sequence of dynamic impacts, designed to be about 200 milliseconds each in duration, was applied on the pier head. After the dynamic PLT test, static tension or compression tests were also performed to evaluate the effect of loading rate. The details of the drilled pier design, installation, and load tests protocol are presented by Kasali and Sitar (2006).

For clarity we present here the test and numerical results of only one of the test piers. The pier is 19 feet (5.8 m) long, 2.5 feet (0.67 m) in diameter. The pier was first loaded dynamically using the PLT device and the dynamic test was followed by a static compression test. The recorded pier head displacement vs. applied axial load for the dynamic PLT and static compression tests is plotted in Fig. 3(a). To allow for better comparison, each PLT cycle and the static curve are re-plotted from the same origin in Fig. 3(b). The data show that the dynamic load-displacement curve has initial stiffness about twice as much as that of the static curve, and it also has higher ultimate strength. The difference between dynamic and static response can be attributed to rate effect of the pile-soil system. Nonlinear load-displacement relationship is pronounced in this plot, and the stiffness of the pile-soil system is dependent on applied load or strain level.

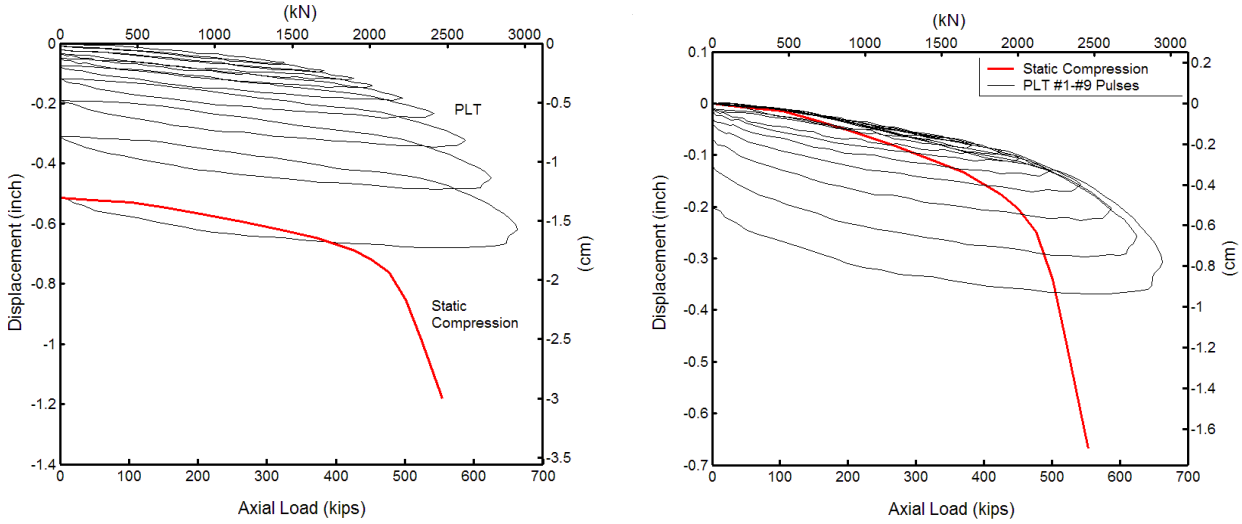

(a) (b)

Figure 3. Dynamic PLT and static compression test

Due to symmetry of the problem, only one half of the soil-pier cross-section was meshed using axisymmetric bilinear element. The finite element mesh, shown in Fig. 4, extends to 40 feet (12.2 m) in depth and 20 feet (6.1 m) in length. The base of the mesh is constrained and only

vertical movement is allowed along the right side of the simulation domain and the axis of symmetry (the left side). The size of the mesh was regarded appropriate for the problem after mesh sensitivity analysis.

Traditionally, frictional contact can be placed along pier-soil interface to allow for slippage between pairs of pier and soil elements. However, field observations reveal that the failure surface of cast-in-place concrete piers does not occur exactly on the material interface, but some distance into the surrounding soil. Instead of utilizing artificial contact elements, the pier and soil elements were assumed perfectly bonded in the analysis presented here. Interface behavior was modeled as plastic yielding through a thin layer of nonlinear soil elements adjacent to the pier shaft. To minimize the bias due to element size, very fine mesh was used in that region.

Important for ensuing analysis, the initial in-situ stress state should be properly developed. A staged loading process was designed to enforce in-situ stress state of soil elements: The soil elements were initially assumed to be linearly elastic, with Poisson's ratio determined by $v = K_0/(1+K_0)$, where K_0 is the coefficient of earth pressure, approximately 0.5 for normally consolidated clays. After vertical consolidation under self-weight to generate the desired K_0 profile, the soil elements were allowed to behave nonlinearly.

The concrete pier was assumed to be linearly elastic. The elastic modulus was assumed 20 GPa, with Poisson's ratio v=0.1 and density $2.4\times10^3 \text{kg/m}^3$. Based on sample test from the site, the soil density was taken as $\rho = 2\times10^3 \text{kg/m}^3$ and Possion's ratio $v = 0.4$. SASW (Spectral Analysis of Surface Waves) measured the average shear velocities $V_s = 289$ m/s over the pier length, so the small strain shear modulus $G_{\max} = \rho V_s^2 = 1.67\times10^5 \text{kPa}$ was computed using this measured value. The undrained shear strength (S_u) profile was estimated from unconfined compression (UC) test, as shown in Fig. 5. The shear strength profile shows fairly high strength of the soil close to the surface, indicating that the soil is overly-consolidated at the top. The high OCR (Over-Consolidation Ratio) may be attributed to desiccation and unloading of overburden pressure during deep excavation when the test site was constructed. To account for loading rate effect, S_u profile used in dynamic case was chosen to be slightly higher than the static case.

The soil modulus reduction and damping factors during cyclic loadings depend on a number of factors including: the amplitude of cyclic strain developed in the soil, as well as plasticity index (PI), void ratio, overconsolidation ratio (OCR), confining pressure, frequency and shape of the cyclic loading-time history etc. For cohesive soils, the plasticity index (PI) has an important influence on the modulus reduction curves (Vucetic and Dobry 1991). With increasing shear strain, clays of higher plasticity indices tend to behave more elastically than low PI soils, resulting in slower rate of modulus reduction and lower damping ratio. Similarly, the modulus of sands reduces much faster than that of clays, and the damping ratio for sands is generally larger. Recent experimental investigations also reveal significant dependence of the form of the modulus reduction curve on the applied strain rate. Due to the rate effect, dynamic and static modulus reduction curves can be quite distinctive especially at small strains. This issue has been examined through comparisons of monotonic and cyclic laboratory tests at varying strain rate (LoPresti. *et*

al. 1996; Shibuya *et al*. 1996). Based on the experiments, the maximum modulus at small strains is not significantly influenced by the imposed strain rate. On the other hand, the elastic threshold strain is influenced by the strain rate, increasing with increasing strain rate. Beyond the elastic threshold strain, the moduli degrade at much faster rate under monotonic loading than under dynamic loading.

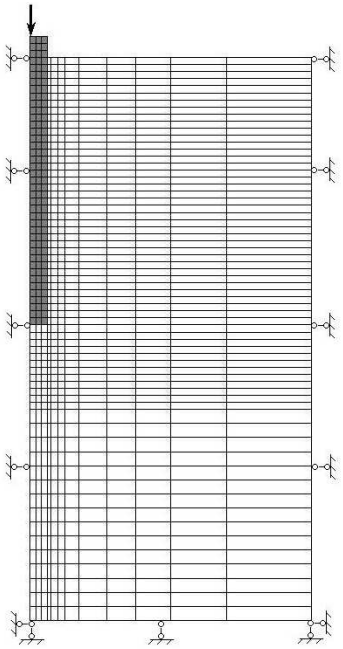

Figure 4. FEM mesh

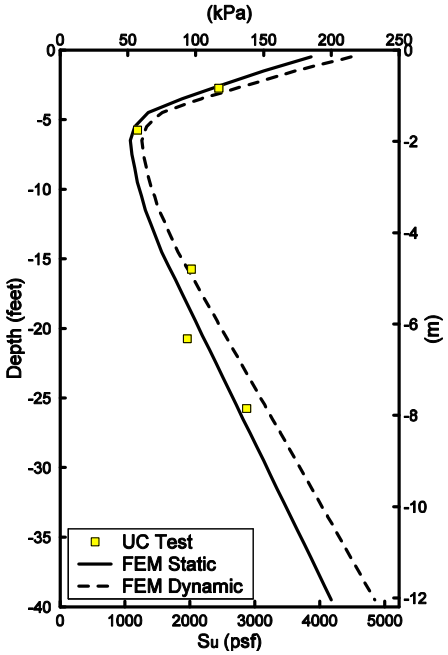

Figure 5. S_u profile

Since the shear modulus reduction curve is rate dependent, different parameters for the static case and dynamic case are used, such that the rate effect can be considered explicitly. As described before, two hardening parameters, *h* and *m*, are used to adjust the shape of the cyclic curves and they can be fitted through the modulus reduction curve of various soil types. Although it is most appropriate to determine the modulus reduction curve on a site-specific basis, with limited site information, the hardening parameters *h* and *m* are chosen to fit the low PI range of Vucetic and Dobry (1991) curves in the dynamic simulation. For the static analysis, we back calculate a static modulus reduction curve, which degrades faster than the dynamic curve. The difference is consistent with that observed in the laboratory tests. The modulus reduction curves used in the analyses are shown in Fig. 6, with the Vucetic and Dobry (1991) curves for PI=0, 15, 30 shown in dashed lines.

Table 2 summarizes soil parameters used for dynamic and static analyses. In the dynamic analyses, very small viscous damping was also used to control the result, and the time step was chosen $\Delta t = 0.005\,\text{sec}$. The predicted PLT curves for pier head displacement versus applied load history are shown in Fig. 7(a), with recorded data in dashed lines for comparison. The plot shows

that the dynamic stiffness of pier-soil system during loading/unloading, the residual displacements, and energy dissipation for all nine cycles can be simulated reasonably well. The overall strength envelope, which encompasses all these cyclic loops, closely follows the observed load displacement loops. It should be noted that during the test, there was considerable rebound at the end of each PLT loop, which cannot be adequately simulated. The lack of rebound accumulates to produce the apparently larger predicted total residual displacement (0.7 inches predicted against 0.5 inches measured).

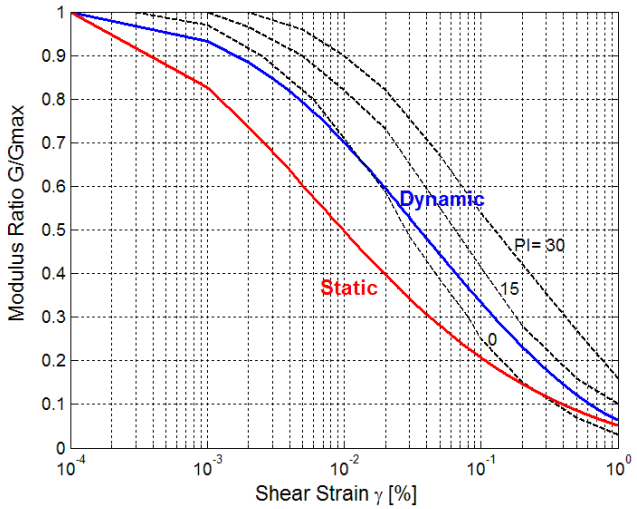

Figure 6. Modulus Reduction Curves

Table 2. Soil Parameters.

	Dynamic	**Static**
ρ	2×10^3kg/m^3	
ν	0.4	
G_{max}	1.67×10^5kPa	
S_u	Profile in Fig. 5	
h	$0.70\,G_{max}$	$0.25\,G_{max}$
m	0.8	
H_0	$G_{max}/300$	0

As described previously, the static compression test was performed after the PLT test. Thus, the PLT load history, i.e. the influence of residual displacement and stress condition, had to be properly taken into account in the finite element analysis. In our static analysis, the pier was first loaded and unloaded to generate the desired residual displacement. The pier was then loaded again and the prediction was compared with the measured data. Fig. 7(b) presents the simulated pier head load displacement response using static soil properties in Table 2. The prediction matches the test data very well for both total response and end bearing component. The compressive load distribution in pier can also be calculated through integration of stresses over Gauss points, as shown in Fig.7 (c). The slope of the distribution curve corresponds to the shear stress of the soil mobilized along the shaft. The deformed mesh (magnified by a factor of 10) at the peak static load can be seen in Fig. 7(d). Although no special interface element was used in this model, the resolution of strain localization is sharp. It is also worth mentioning that, although the displacement gradient is highly concentrated close to the shaft, the maximum shear strain developed in these elements reaches only about 3%.

Conclusions

Rate effect of cyclic loading can lead up to 100% increase in stiffness and 40% increase in capacity of a pier-soil system compared to the static loading; The nonlinear finite element and cyclic soil model we developed has successfully captured the pier-soil system stiffness, capacity

and energy dissipation through simulation of a prototype pier under dynamic and static axial loading tests. The general performance of the model is robust and reasonably fast. For example, the total run time was approximately 12 minutes for a full analysis consisting of 789 elements and 540 time steps on a personal computer (Pentium IV 2G Hz CPU). The nonlinear cyclic soil model has been implemented in an open source finite element framework (OpenSees), and it shows great promise for future use in three-dimensional fully coupled nonlinear soil-structure analyses.

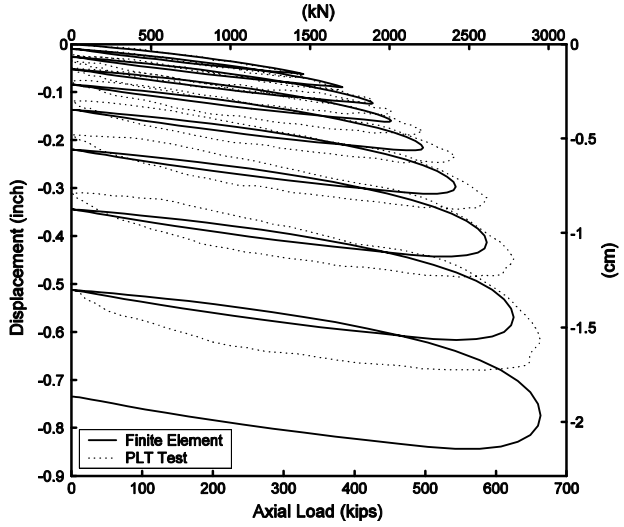

(a) Dynamic PLT simulation

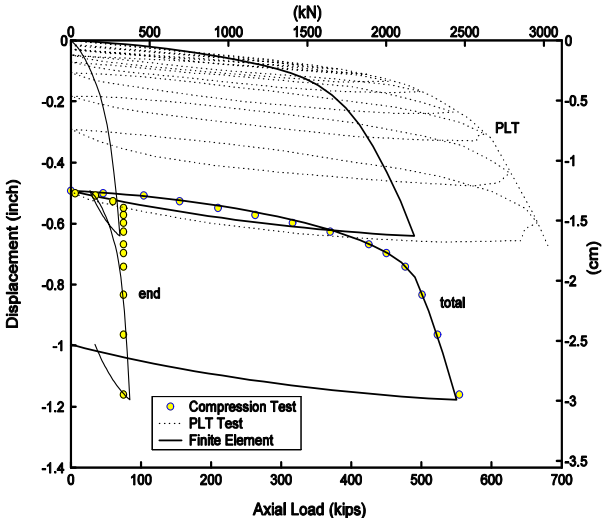

(b) Static compression simulation

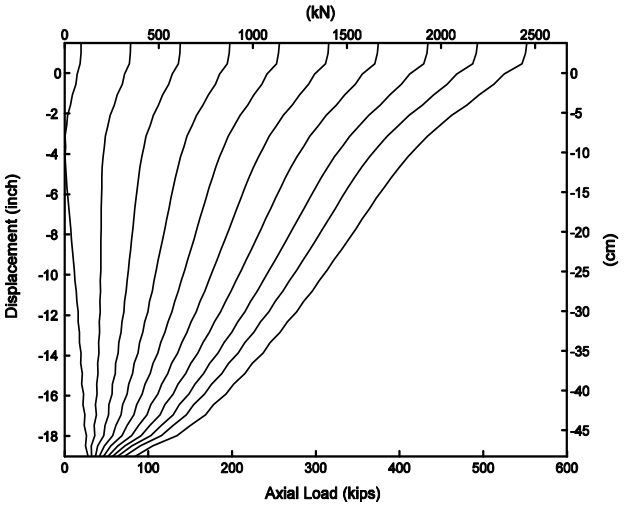

(c) Compressive load distribution

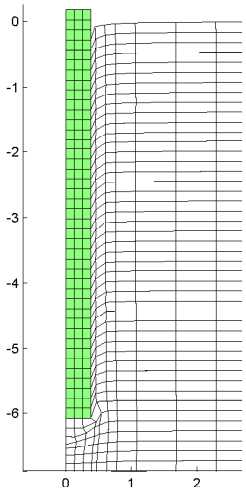

(d) Deformed mesh ($\times 10$)

Figure 7. Finite element simulation results

Acknowledgments

Financial support from Pacific Earthquake Engineering Research Center (PEER) through NSF Award NO. EEC-9701568 is gracefully acknowledged.

References

Borja, R.I., and A.P. Amies, 1994. Multiaxial cyclic plasticity model, *ASCE Journal of Geotechnical Engineering* 120 (6), 1051-1070.

Borja, R.I., H. Chao, F.J. Montans, and CH. Lin, 1999a. Nonlinear ground response at Lotung LSST site, *ASCE Journal of Geotechnical and Geoenvironmental Engineering* 125 (3), 187-197.

Borja, R.I., H. Chao, F.J. Montans, and CH. Lin, 1999b. SSI effects on ground motion at Lotung LSST site, *ASCE Journal of Geotechnical and Geoenvironmental Engineering* 125 (9), 760-770.

Kasali, G., and N. Sitar, 2006. Field evaluation of axial response of drilled shafts to dynamic loads. *Proceedings, Eighth US National Conference on Earthquake Engineering*, San Francisco.

Kraft, L. M., W.R. Cox, and E.A. Verner, 1981. Pile load tests – cyclic loads and varying load tests. *ASCE Journal of Geotechnical Engineering Division* 107 (1), 1-19.

LoPresti, D.C.F., M. Jamiolkowski, O. Pallara and A. Cavallaro, 1996. Rate and creep effect on the stiffness of soils, *ASCE Geotechnical Special Publication* 61, 166-180.

OpenSees ©. *Open System for Earthquake Engineering Simulation*, University of California, Berkeley. http://opensees.berkeley.edu

Potts, D.M., and L. Zdravkovic, 1999, 2001. *Finite Element Analysis in Geotechnical Engineering, Vol. 1: Theory, Vol. 2: Application*. Thomas Telford Publishing.

Rodriguez-Marek, A., 2000. Near-fault seismic site response, *Ph.D. Thesis*, University of California, Berkeley.

Shibuya, S., T. Mitachi, A. Hosomi, and S.C. Hwang, 1996. Strain rate effects on stress-strain behaviour of clay as observed in monotonic and cyclic triaxial tests. *ASCE Geotechnical Special Publication* 61, 214-227.

Vucetic, M., and R. Dobry, 1991. Effect of soil plasticity on cyclic response, *ASCE Journal of Geotechnical Engineering Division* 117 (1), 89-107.

Wang, G., 2005. Nonlinear analysis of a drilled pier-soil system under static and dynamic axial loading, *Ph.D. Thesis*, University of California, Berkeley.

Zienkiewicz, O. C., A. H. C. Chan, M. Pastor, B. A. Schrefler and T. Shiomi, 1999. *Computational Geomechanics with Special Reference to Earthquake Engineering.* John Wiley & Sons.